

k·p method for strained wurtzite semiconductors

S. L. Chuang and C. S. Chang

*Department of Electrical and Computer Engineering, University of Illinois at Urbana-Champaign,
1406 West Green Street, Urbana, Illinois 61801*

(Received 24 January 1996)

We derive the effective-mass Hamiltonian for wurtzite semiconductors, including the strain effects. This Hamiltonian provides a theoretical groundwork for calculating the electronic band structures and optical constants of bulk and quantum-well wurtzite semiconductors. We apply Kane's model to derive the band-edge energies and the optical momentum-matrix elements for strained wurtzite semiconductors. We then use the **k·p** perturbation method to derive the effective-mass Hamiltonian, which is then checked with that derived using an invariant method based on the Pikus-Bir model. We obtain the band structure A_i parameters in the group theoretical model explicitly in terms of the momentum-matrix elements. We also find the proper definitions of the important physical quantities used in both models and present analytical expressions for the valence-band dispersions, the effective masses, and the interband optical-transition momentum-matrix elements near the band edges, taking into account the strain effects. [S0163-1829(96)00428-6]

I. INTRODUCTION

Wide band-gap semiconductors including GaN, AlN, InN, and their ternary compounds have recently received considerable attention.¹⁻⁶ The worldwide competition for fabricating blue-green laser diodes following the success of high-brightness blue-green light-emitting diodes and other applications of these materials for electronic devices generate an intensive research effort on the growth and characterization of the nitride based semiconductors.

Since these group-III nitrides crystallize in the wurtzite structure when grown in the most common substrates, such as a sapphire (0001) substrate, fundamental studies of the wurtzite band structure play an important role in understanding the electronic and optical properties of GaN based optoelectronic materials and devices. Although GaN wurtzite structures were investigated in the 1960s,^{7,8} most theoretical⁹⁻²¹ and experimental studies^{3-5,22} of these wurtzite materials increased dramatically in the 1990s after the demonstration of the light-emitting diodes using the GaN/Al_xGa_{1-x}N semiconductors.^{1,2}

Full band-structure calculations have been reported for binary⁹⁻¹⁴ and ternary¹⁸⁻²¹ semiconductors with wurtzite structures. For electronic and optical properties, the band structure near the direct band edges can be used to understand experimental observations such as the photoluminescence spectrum and mobility measurements. The Hamiltonian near the band edge of a wurtzite semiconductor has been derived using an invariant method,^{7,8} and many of the band-structure parameters were treated empirically with little indication of the origin of these parameters. First-principle calculations may be applied to calculate the band-structure parameters, the splitting energies (Δ_i), and the deformation potentials. Unfortunately, many parameters (such as the crystal-field splitting energy, the spin-orbit split-off energies, the band-edge effective-mass parameters, and especially the deformation potentials) are not readily available¹⁸⁻²¹ from the full band-structure calculations for wurtzite structures. The band-structure parameters have only recently been ex-

tracted by fitting the band-edge dispersion curves with those calculated by the more accurate self-consistent full-potential linearized-augmented plane-wave method within the local-density-functional approximation.¹⁴ Yet, these theoretical parameters, especially Δ_1 and D_i s, appear to be too big when they are compared with the experimental data in Ref. 23. On the other hand, the band structures of zinc-blende semiconductors near the band edge are usually derived using the **k·p** method or the Luttinger-Kohn model.²⁴⁻²⁶ The parameters in the Luttinger-Kohn model are clearly defined in terms of physical quantities, such as momentum-matrix elements and eigenenergies. In this paper, we present a derivation of the Hamiltonian matrix for wurtzite structures based on the **k·p** method and show the explicit definitions of the band-structure parameters and interband optical momentum-matrix elements. Many of the analytical expressions including strain effects are derived. Since current GaN heterojunction structures have a significant amount of strain, these results will be valuable to researchers in this field. Our presentation also clarifies some inconsistencies in the earlier papers, due to ambiguities in the choices of the basis functions and the change of definitions in the operators used in the invariant method in different papers.

In Sec. II, we present Kane's model²⁴ for wurtzite band structures and define the band-edge parameters, such as the crystal-field splitting energy and the spin-orbit energy, and the interband momentum-matrix elements for the $x(=y)$ and z polarizations, where the z axis is chosen to be the c axis (0001) of the wurtzite structure. The wurtzite structure, Fig. 1, consists of two interpenetrating hexagonal closely packed sublattices, offset along the c axis (z axis) by $5/8$ of the cell height c . The sixfold rotation symmetry is used in deriving some of the fundamental physical parameters. In Sec. III, we derive the Hamiltonian matrix based on the Luttinger-Kohn model and find the explicit definitions of the band-structure parameters. These band-structure parameters are then related to those parameters A_1, A_2, \dots, A_6 , used in the Hamiltonian matrix derived with the invariant method, presented in Sec. IV. Using the property that these band-structure parameters are real, we are able to identify the proper choice of the phase factor in the corresponding set of basis functions and

operators in the Hamiltonian. In Sec. V, we found that the six-by-six Hamiltonian can be block diagonalized to two three-by-three matrices following a unitary transformation of the basis functions. In Sec. VI, we show analytical expressions for the effective masses near and away from the zone center and the interband optical-transition matrix elements, taking into account the strain effects. Numerical examples for GaN and AlN are shown in Sec. VII and the conclusions are given in Sec. VIII. We hope that our analysis not only shows a consistent and clear derivation of the Hamiltonian for wurtzite crystals, but also stimulates more fundamental studies and measurements of the band-edge electronic parameters and optical-transition oscillator strengths.

II. KANE'S MODEL FOR WURTZITE SEMICONDUCTORS

In this section, we use Kane's model²⁴ to find the band-edge energies and define important physical parameters including the optical momentum-matrix elements.

A. The Hamiltonian matrix elements

The Schrödinger equation for the periodic part $u_{n\mathbf{k}}(\mathbf{r})$ of the Bloch function and the energy $E_n(\mathbf{k})$ near the band edge can be written as^{24,26}

$$\begin{aligned} H u_{n\mathbf{k}}(\mathbf{r}) &\simeq \left(H_0 + \frac{\hbar^2 k^2}{2m_0} + \frac{\hbar}{m_0} \mathbf{k} \cdot \mathbf{p} + H_{so} \right) u_{n\mathbf{k}}(\mathbf{r}) \\ &= E_n(\mathbf{k}) u_{n\mathbf{k}}(\mathbf{r}), \end{aligned} \quad (1)$$

where

$$H_0 = \frac{p^2}{2m_0} + V(\mathbf{r}), \quad (2)$$

$$H_{so} = \frac{\hbar}{4m_0^2 c^2} \nabla V \times \mathbf{p} \cdot \boldsymbol{\sigma} = H_{sx} \sigma_x + H_{sy} \sigma_y + H_{sz} \sigma_z. \quad (3)$$

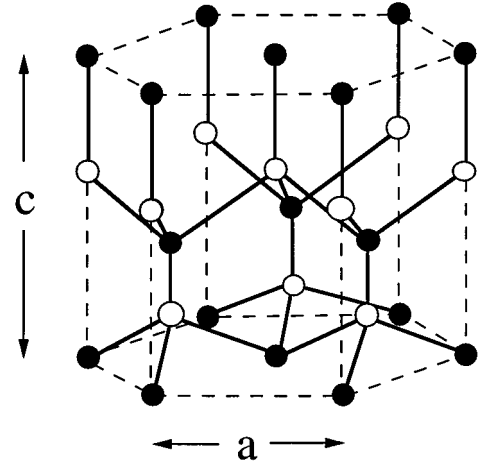


FIG. 1. A wurtzite crystal consists of two interpenetrating hexagonal closely packed sublattices, displaced by $5/8$ of the $c(0001)$ axis. The dashed lines show the boundary of a unit cell.

Here, $V(\mathbf{r})$ is the periodic potential, H_{so} accounts for the spin-orbit interaction, and $\sigma_i, i=x,y,z$ are the Pauli spin matrices, which are defined in Appendix A.

In the set of basis functions near the zone center,

$$\begin{aligned} |iS\uparrow\rangle, \quad u_1 &= \left| -\frac{(X+iY)}{\sqrt{2}} \uparrow \right\rangle, \quad u_2 = \left| \frac{(X-iY)}{\sqrt{2}} \uparrow \right\rangle, \\ u_3 &= |Z\uparrow\rangle; \\ |iS\downarrow\rangle, \quad u_4 &= \left| \frac{(X-iY)}{\sqrt{2}} \downarrow \right\rangle, \quad u_5 = \left| -\frac{(X+iY)}{\sqrt{2}} \downarrow \right\rangle, \\ u_6 &= |Z\downarrow\rangle. \end{aligned} \quad (4)$$

The Hamiltonian matrix can be written in the following form:

$$H_{8 \times 8} = \frac{\hbar^2 k^2}{2m_0} + \begin{bmatrix} E_c & -\frac{k_+ P_2}{\sqrt{2}} & \frac{k_- P_2}{\sqrt{2}} & k_z P_1 & 0 & 0 & 0 & 0 \\ -\frac{k_- P_2}{\sqrt{2}} & E_v + \Delta_1 + \Delta_2 & 0 & 0 & 0 & 0 & 0 & 0 \\ \frac{k_+ P_2}{\sqrt{2}} & 0 & E_v + \Delta_1 - \Delta_2 & 0 & 0 & 0 & 0 & \sqrt{2} \Delta_3 \\ k_z P_1 & 0 & 0 & E_v & 0 & 0 & \sqrt{2} \Delta_3 & 0 \\ 0 & 0 & 0 & 0 & E_c & \frac{k_- P_2}{\sqrt{2}} & -\frac{k_+ P_2}{\sqrt{2}} & k_z P_1 \\ 0 & 0 & 0 & 0 & \frac{k_+ P_2}{\sqrt{2}} & E_v + \Delta_1 + \Delta_2 & 0 & 0 \\ 0 & 0 & 0 & \sqrt{2} \Delta_3 & -\frac{k_- P_2}{\sqrt{2}} & 0 & E_v + \Delta_1 - \Delta_2 & 0 \\ 0 & 0 & \sqrt{2} \Delta_3 & 0 & k_z P_1 & 0 & 0 & E_v \end{bmatrix}, \quad (5)$$

where

$$k_{\pm} = k_x \pm ik_y \quad (6)$$

and we have used the following definitions for the energies:

$$\begin{aligned} \langle S|H_0|S\rangle &= E_c, \\ \langle X|H_0|X\rangle &= \langle Y|H_0|Y\rangle = E_v + \Delta_1, \\ \langle Z|H_0|Z\rangle &= E_v, \\ \langle X|H_{sz}|Y\rangle &= -i\Delta_2, \\ \langle Y|H_{sx}|Z\rangle &= \langle Z|H_{sy}|X\rangle = -i\Delta_3, \end{aligned} \quad (7)$$

and two Kane's parameters, P_1 and P_2 , which are related to the interband momentum-matrix elements,

$$\begin{aligned} \left\langle iS \left| \frac{\hbar}{i} \frac{\partial}{\partial z} \right| Z \right\rangle &= \frac{m_0}{\hbar} P_1, \\ \left\langle iS \left| \frac{\hbar}{i} \frac{\partial}{\partial x} \right| X \right\rangle &= \left\langle iS \left| \frac{\hbar}{i} \frac{\partial}{\partial y} \right| Y \right\rangle = \frac{m_0}{\hbar} P_2. \end{aligned} \quad (8)$$

Note that in the original Kane's model for cubic crystals, the wave vector \mathbf{k} is assumed to be along the z direction, which is possible due to the cubic symmetry. For wurtzite crystals, we have to keep all three components of the \mathbf{k} vector. In the derivations of the matrix elements, the sixfold symmetry on

the x - y plane has been used. For example, (x, y) mapping to a 60° rotation around the z axis ($=c$ axis) leaves the Hamiltonian invariant, and the wave functions $|X\rangle$ and $|Y\rangle$ transform to

$$\begin{aligned} |X'\rangle &= \frac{1}{2}|X\rangle + \frac{\sqrt{3}}{2}|Y\rangle, \\ |Y'\rangle &= -\frac{\sqrt{3}}{2}|X\rangle + \frac{1}{2}|Y\rangle. \end{aligned} \quad (9)$$

Therefore,

$$\langle Y|H_0|Y\rangle = \langle Y'|H_0|Y'\rangle = \frac{3}{4}\langle X|H_0|X\rangle + \frac{1}{4}\langle Y|H_0|Y\rangle \quad (10)$$

and we find $\langle Y|H_0|Y\rangle = \langle X|H_0|X\rangle$. We also obtain $\langle X|H_0|Y\rangle = 0$, and $\langle S|H_0|X\rangle = 0$. The properties $\langle S|\partial/\partial x|X\rangle = \langle S|\partial/\partial y|Y\rangle$ and $\langle Y|H_{sx}|Z\rangle = \langle Z|H_{sy}|X\rangle$ can be derived in a similar manner.

B. Band-edge energies and basis functions

At the zone center, we obtain the doubly degenerate band-edge energies with their corresponding basis functions from the eigenvalues and eigenvectors of the Hamiltonian in Eq. (5) at $k_x = k_y = k_z = 0$.

$$\begin{aligned} & E_c, & |iS\uparrow\rangle, & |iS\downarrow\rangle, \\ & E_1 = E_v + \Delta_1 + \Delta_2, & u_1, & u_4, \\ E_2 = E_v + \frac{\Delta_1 - \Delta_2}{2} + \sqrt{\left(\frac{\Delta_1 - \Delta_2}{2}\right)^2 + 2\Delta_3^2}, & au_2 + bu_6, & bu_3 + au_5, \\ E_3 = E_v + \frac{\Delta_1 - \Delta_2}{2} - \sqrt{\left(\frac{\Delta_1 - \Delta_2}{2}\right)^2 + 2\Delta_3^2}, & bu_2 - au_6, & -au_3 + bu_5, \end{aligned} \quad (11)$$

where

$$a = \frac{E_2}{\sqrt{E_2^2 + 2\Delta_3^2}}, \quad b = \frac{\sqrt{2}\Delta_3}{\sqrt{E_2^2 + 2\Delta_3^2}} \quad (12)$$

and the reference energy has been set at $E_v = 0$ in (12), for convenience. The band-edge energies can also be described by considering the following simplified case. If without the spin-orbit interaction effects, $\Delta_2 = \Delta_3 = 0$, we have $E_1 = E_2 = \Delta_1$, and $E_3 = 0$ (for a positive Δ_1), as shown in Fig. 2(a). When we include a nonvanishing $\Delta_2 = \Delta_3$ to take into account the spin-orbit interaction, Fig. 2(b) shows the energy splittings. For GaN, Δ_1 is positive, the top valence-band energy is E_1 , and the band-gap energy is $E_c - E_1 = E_g$. Therefore, the conduction-band edge energy is $E_c = E_g + \Delta_1 + \Delta_2$, measured from the reference energy $E_v = 0$ of GaN. The band-edge energies are summarized in Fig. 2(b). The three bands are labeled according to their zone center wave functions. In general, if $\Delta_1 > \Delta_2 > 0$, the three

bands from top to bottom can be labeled as heavy-hole (HH), light-hole (LH), and crystal-field split-off hole (CH) bands, respectively. We can relate these energies to the crystal-field split energy, Δ_{cr} , and the spin-orbit split-off energy, Δ_{so} , by

$$\Delta_1 = \Delta_{cr}, \quad \Delta_2 = \Delta_3 = \frac{1}{3}\Delta_{so}. \quad (13)$$

The energy splittings $E_1 - E_2$ and $E_1 - E_3$ are measured²⁷ from the differences between the interband optical-transition energies,

$$\begin{aligned} E_1 - E_2 &= \frac{1}{2} \left(\Delta_{cr} + \Delta_{so} - \sqrt{(\Delta_{cr} + \Delta_{so})^2 - \frac{8}{3}\Delta_{cr}\Delta_{so}} \right), \\ E_1 - E_3 &= \frac{1}{2} \left(\Delta_{cr} + \Delta_{so} + \sqrt{(\Delta_{cr} + \Delta_{so})^2 - \frac{8}{3}\Delta_{cr}\Delta_{so}} \right), \end{aligned} \quad (14)$$

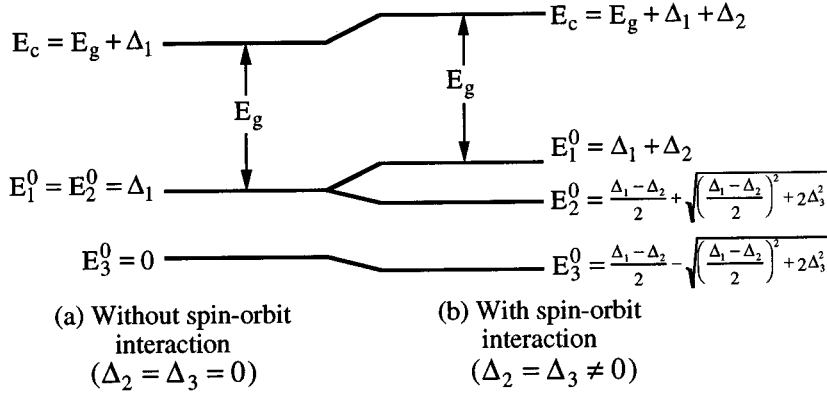


FIG. 2. The band-edge energies (a) without spin-orbit interaction ($\Delta_2 = \Delta_3 = 0$) and (b) with spin-orbit interaction ($\Delta_2 = \Delta_3 \neq 0$) for GaN wurtzite semiconductor. The corresponding band-edge energies are also listed.

which then determine the values of Δ_{cr} and Δ_{so} . Since the solutions are symmetric with respect to these two parameters, extra procedures such as measuring the polarization selection rules in the optical transitions from the conduction band to the three valence bands or the theoretical approach to calculate the full valence-band structures are needed to determine these parameters. Note that in the above two equations, Eqs. (13) and (14), the cubic approximation [Eq. (36)] has been used. A reported theoretical value¹⁴ of 72.9 meV for Δ_{cr} of GaN seems to be too big compared with the available experimental data ranging from the commonly used value²⁷ of 22 meV to the recently reported value²³ of 10 meV.

On the other hand, for AlN, Δ_1 is negative, the top valence band is E_2 , and the conduction-band energy is $E_c = E_g + E_2$ measured from the reference energy E_v of AlN. The valence bands from top to bottom are CH, LH, and HH, respectively.

C. Optical momentum-matrix elements

The determinant of the 8×8 matrix gives the energy dispersion relation

$$\begin{aligned}
 0 &= \det(H_{8 \times 8} - EI_{8 \times 8}) \\
 &= \{-(E_c - E')(E_v + \Delta_1 + \Delta_2 - E') \\
 &\quad \times [(E_v + \Delta_1 - \Delta_2 - E')(E_v - E') - 2\Delta_3^2] \\
 &\quad + [(E_v + \Delta_1 - E')(E_v - E') - \Delta_3^2]P_2^2(k_x^2 + k_y^2) \\
 &\quad + (E_v + \Delta_1 + \Delta_2 - E')(E_v + \Delta_1 - \Delta_2 - E')P_1^2k_z^2\}^2,
 \end{aligned} \tag{15}$$

where $E' = E - (\hbar^2 k^2 / 2m_0)$. If we focus on the eigenvalue near the conduction-band edge with a small k value, we find from Eq. (15) the conduction-band dispersion relation,

$$\begin{aligned}
 E(\mathbf{k}) &= E_c + \frac{\hbar^2 k^2}{2m_0} + \frac{(E_g + \Delta_1 + \Delta_2)(E_g + \Delta_2) - \Delta_3^2}{E_g[(E_g + \Delta_1 + \Delta_2)(E_g + 2\Delta_2) - 2\Delta_3^2]} \\
 &\quad \times P_2^2(k_x^2 + k_y^2) \\
 &\quad + \frac{(E_g + 2\Delta_2)}{(E_g + \Delta_1 + \Delta_2)(E_g + 2\Delta_2) - 2\Delta_3^2} P_1^2 k_z^2,
 \end{aligned} \tag{16}$$

which can also be written in terms of the transverse and longitudinal effective masses.

$$E(\mathbf{k}) = E_c + \frac{\hbar^2(k_x^2 + k_y^2)}{2m_e^t} + \frac{\hbar^2 k_z^2}{2m_e^z}. \tag{17}$$

Then, we obtain the Kane's parameters,

$$\begin{aligned}
 P_1^2 &= \frac{\hbar^2}{2m_0} \left(\frac{m_0}{m_e^z} - 1 \right) \frac{(E_g + \Delta_1 + \Delta_2)(E_g + 2\Delta_2) - 2\Delta_3^2}{(E_g + 2\Delta_2)}, \\
 P_2^2 &= \frac{\hbar^2}{2m_0} \left(\frac{m_0}{m_e^t} - 1 \right) \frac{E_g[(E_g + \Delta_1 + \Delta_2)(E_g + 2\Delta_2) - 2\Delta_3^2]}{(E_g + \Delta_1 + \Delta_2)(E_g + \Delta_2) - \Delta_3^2},
 \end{aligned} \tag{18}$$

which are related directly to the optical momentum-matrix elements in Eq. (8).

III. THE $\mathbf{k} \cdot \mathbf{p}$ METHOD FOR STRAINED WURTZITE SEMICONDUCTORS

When a few bands are close to each other in energy levels, the perturbation theory for degenerate bands has to be used. An improved method is the so-called Löwdin's perturbation method,^{28,26} which provides the Hamiltonian to the second order in the $\mathbf{k} \cdot \mathbf{p}$ contributions.

A. General formulation

We write the total Hamiltonian as²⁶

$$\begin{aligned}
 Hu_{\mathbf{k}}(\mathbf{r}) &= E(\mathbf{k})u_{\mathbf{k}}(\mathbf{r}), \\
 H &= H_0 + \frac{\hbar^2 k^2}{2m_0} + H_{so} + H',
 \end{aligned} \tag{19}$$

where

$$\begin{aligned}
 H' &= \frac{\hbar}{m_0} \mathbf{k} \cdot \mathbf{\Pi}, \\
 \mathbf{\Pi} &= \mathbf{p} + \frac{\hbar}{4m_0 c^2} \boldsymbol{\sigma} \times \nabla V.
 \end{aligned} \tag{20}$$

It is noted that the last term in $\mathbf{\Pi}$ is usually neglected for simplicity.^{8,26} The band-edge wave function can be written as

$$u_{\mathbf{k}}(\mathbf{r}) = \sum_{j'}^A a_{j'}(\mathbf{k}) u_{j'0}(\mathbf{r}) + \sum_{\gamma}^B a_{\gamma}(\mathbf{k}) u_{\gamma 0}(\mathbf{r}) \tag{21}$$

and we choose the six valence-band wave functions, $\{u_1, u_2, \dots, u_6\}$ in Eq. (4), as the bases for the states of interest (called class A), and all other states of no interest are called class B .

$$\begin{aligned}
 |u_1\rangle &= \frac{-1}{\sqrt{2}}|(X+iY)\uparrow\rangle, \\
 |u_2\rangle &= \frac{1}{\sqrt{2}}|(X-iY)\uparrow\rangle, \\
 |u_3\rangle &= |Z\uparrow\rangle, \\
 |u_4\rangle &= \frac{1}{\sqrt{2}}|(X-iY)\downarrow\rangle, \\
 |u_5\rangle &= \frac{-1}{\sqrt{2}}|(X+iY)\downarrow\rangle, \\
 |u_6\rangle &= |Z\downarrow\rangle.
 \end{aligned} \tag{22}$$

Using Löwdin's method,²⁸ the six-by-six Hamiltonian matrix for the valence bands can be written as the sum of a band-edge contribution and a \mathbf{k} -dependent contribution.

$$H_{6 \times 6, jj'}(\mathbf{k}) = H_{6 \times 6, jj'}(\mathbf{k}=0) + D_{jj'} \tag{23}$$

and the \mathbf{k} -dependent matrix is

$$\begin{aligned}
 D_{jj'} &= \sum_{\alpha, \beta} D_{jj'}^{\alpha\beta} k_{\alpha} k_{\beta}, \\
 D_{jj'}^{\alpha\beta} &= \frac{\hbar^2}{2m_0} \left[\delta_{jj'} \delta_{\alpha\beta} + \sum_{\gamma} \frac{P_{j\gamma}^{\alpha} P_{\gamma j'}^{\beta} + P_{j\gamma}^{\beta} P_{\gamma j'}^{\alpha}}{m_0(E_0 - E_{\gamma})} \right], \tag{24}
 \end{aligned}$$

where the indices $j, j' = 1, 2, \dots, 6 \in A$, $\gamma \in B$, and $\alpha, \beta = x, y, z$. The band-edge Hamiltonian matrix has been obtained from Kane's model,

$$H_{6 \times 6}(\mathbf{k}=0) = \begin{bmatrix} E_v + \Delta_1 + \Delta_2 & 0 & 0 & 0 & 0 & 0 \\ 0 & E_v + \Delta_1 - \Delta_2 & 0 & 0 & 0 & \sqrt{2}\Delta_3 \\ 0 & 0 & E_v & 0 & \sqrt{2}\Delta_3 & 0 \\ 0 & 0 & 0 & E_v + \Delta_1 + \Delta_2 & 0 & 0 \\ 0 & 0 & \sqrt{2}\Delta_3 & 0 & E_v + \Delta_1 - \Delta_2 & 0 \\ 0 & \sqrt{2}\Delta_3 & 0 & 0 & 0 & E_v \end{bmatrix}. \tag{25}$$

B. The D matrix in the $|X\rangle$, $|Y\rangle$, and $|Z\rangle$ bases

First, we use a method similar to that of the Luttinger-Kohn paper²⁵ to define a few fundamental band-structure parameters, L_1 , L_2 , M_1 , M_2 , M_3 , N_1 , and N_2 . The 3×3 matrix with components, $D_{ij}, i, j = X, Y, Z$, can be written in the following form:

$$D_{3 \times 3} = \begin{bmatrix} L_1 k_x^2 + M_1 k_y^2 + M_2 k_z^2 & N_1 k_x k_y & N_2 k_x k_z \\ N_1 k_x k_y & M_1 k_x^2 + L_1 k_y^2 + M_2 k_z^2 & N_2 k_y k_z \\ N_2 k_x k_z & N_2 k_y k_z & M_3 (k_x^2 + k_y^2) + L_2 k_z^2 \end{bmatrix} \begin{matrix} |X\rangle \\ |Y\rangle \\ |Z\rangle \end{matrix}, \tag{26}$$

where we have defined the band-structure parameters, which are similar to the Luttinger-Kohn parameters γ_1 , γ_2 , and γ_3 for zinc-blende structures,

$$\begin{aligned}
 L_1 &= \frac{\hbar^2}{2m_0} \left(1 + \sum_{\gamma}^B \frac{2P_{X\gamma}^x P_{\gamma X}^x}{m_0(E_0 - E_{\gamma})} \right) \\
 &= \frac{\hbar^2}{2m_0} \left(1 + \sum_{\gamma}^B \frac{2P_{Y\gamma}^y P_{\gamma Y}^y}{m_0(E_0 - E_{\gamma})} \right), \\
 L_2 &= \frac{\hbar^2}{2m_0} \left(1 + \sum_{\gamma}^B \frac{2P_{Z\gamma}^z P_{\gamma Z}^z}{m_0(E_0 - E_{\gamma})} \right),
 \end{aligned}$$

$$\begin{aligned}
 M_1 &= \frac{\hbar^2}{2m_0} \left(1 + \sum_{\gamma}^B \frac{2P_{X\gamma}^y P_{\gamma X}^y}{m_0(E_0 - E_{\gamma})} \right) \\
 &= \frac{\hbar^2}{2m_0} \left(1 + \sum_{\gamma}^B \frac{2P_{Y\gamma}^x P_{\gamma Y}^x}{m_0(E_0 - E_{\gamma})} \right), \\
 M_2 &= \frac{\hbar^2}{2m_0} \left(1 + \sum_{\gamma}^B \frac{2P_{X\gamma}^z P_{\gamma X}^z}{m_0(E_0 - E_{\gamma})} \right) \\
 &= \frac{\hbar^2}{2m_0} \left(1 + \sum_{\gamma}^B \frac{2P_{Y\gamma}^z P_{\gamma Y}^z}{m_0(E_0 - E_{\gamma})} \right), \tag{27}
 \end{aligned}$$

$$M_3 = \frac{\hbar^2}{2m_0} \left(1 + \sum_{\gamma}^B \frac{2p_{Z\gamma}^x p_{\gamma Z}^x}{m_0(E_0 - E_{\gamma})} \right)$$

$$= \frac{\hbar^2}{2m_0} \left(1 + \sum_{\gamma}^B \frac{2p_{Z\gamma}^y p_{\gamma Z}^y}{m_0(E_0 - E_{\gamma})} \right),$$

$$N_1 = \frac{\hbar^2}{m_0^2} \sum_{\gamma}^B \frac{p_{X\gamma}^x p_{\gamma Y}^y + p_{X\gamma}^y p_{\gamma Y}^x}{(E_0 - E_{\gamma})},$$

$$N_2 = \frac{\hbar^2}{m_0^2} \sum_{\gamma}^B \frac{p_{X\gamma}^x p_{\gamma Z}^z + p_{X\gamma}^z p_{\gamma Z}^x}{(E_0 - E_{\gamma})} = \frac{\hbar^2}{m_0^2} \sum_{\gamma}^B \frac{p_{Y\gamma}^y p_{\gamma Z}^z + p_{Y\gamma}^z p_{\gamma Z}^y}{(E_0 - E_{\gamma})},$$

where $p_{X\gamma}^y = \langle X | p^y | \gamma \rangle$, etc., and $p^y = (\hbar/i)(\partial/\partial y)$ is the y component of the momentum operator.

C. The six-by-six Hamiltonian matrix in the bases $\{u_1, u_2, \dots, u_6\}$

Using the results in Sec. III B, the $D_{6 \times 6}$ matrix in the bases $\{u_1, u_2, \dots, u_6\}$ can be easily derived using the matrix elements, D_{XX} , D_{XY} , D_{XZ} , etc. in Eq. (26),

$$D_{6 \times 6} = \begin{bmatrix} D_{11} & D_{21}^* & -D_{23}^* & & & \\ D_{21} & D_{11} & D_{23} & & & 0 \\ -D_{23} & D_{23}^* & D_{ZZ} & & & \\ & & & D_{11} & D_{21} & D_{23} \\ & & & & D_{21}^* & D_{11} & -D_{23}^* \\ & & & & D_{23}^* & -D_{23} & D_{ZZ} \end{bmatrix}, \quad (28)$$

where the whole matrix can be expressed by using only four distinctive matrix elements,

$$D_{11} = \left(\frac{L_1 + M_1}{2} \right) (k_x^2 + k_y^2) + M_2 k_z^2,$$

$$D_{ZZ} = M_3 (k_x^2 + k_y^2) + L_2 k_z^2,$$

$$D_{21} = -\frac{1}{2} [(L_1 - M_1)(k_x^2 - k_y^2) + 2iN_1 k_x k_y]$$

$$= -\frac{1}{2} N_1 (k_x + ik_y)^2, \quad (29)$$

$$D_{23} = \frac{1}{\sqrt{2}} N_2 (k_x + ik_y) k_z,$$

and it can be shown (see Appendix B) from symmetry consideration that

$$L_1 - M_1 = N_1. \quad (30)$$

The full Hamiltonian, $H = H_{6 \times 6}(\mathbf{k}=0) + D_{6 \times 6}$, can be written as

$$H = \begin{bmatrix} F & -K^* & -H^* & 0 & 0 & 0 \\ -K & G & H & 0 & 0 & \Delta \\ -H & H^* & \lambda & 0 & \Delta & 0 \\ 0 & 0 & 0 & F & -K & H \\ 0 & 0 & \Delta & -K^* & G & -H^* \\ 0 & \Delta & 0 & H^* & -H & \lambda \end{bmatrix} \begin{bmatrix} |u_1\rangle \\ |u_2\rangle \\ |u_3\rangle \\ |u_4\rangle \\ |u_5\rangle \\ |u_6\rangle \end{bmatrix}, \quad (31)$$

where

$$F = \Delta_1 + \Delta_2 + \lambda + \theta,$$

$$G = \Delta_1 - \Delta_2 + \lambda + \theta,$$

$$\lambda = \frac{\hbar^2}{2m_0} [A_1 k_z^2 + A_2 (k_x^2 + k_y^2)],$$

$$\theta = \frac{\hbar^2}{2m_0} [A_3 k_z^2 + A_4 (k_x^2 + k_y^2)], \quad (32)$$

$$K = \frac{\hbar^2}{2m_0} A_5 (k_x + ik_y)^2,$$

$$H = \frac{\hbar^2}{2m_0} A_6 (k_x + ik_y) k_z,$$

$$\Delta = \sqrt{2} \Delta_3.$$

We obtain the relations between the band-structure parameters derived using the $\mathbf{k} \cdot \mathbf{p}$ method and the more commonly used A_i parameters in the Pikus-Bir model,

$$\frac{\hbar^2}{2m_0} A_1 = L_2, \quad \frac{\hbar^2}{2m_0} A_2 = M_3, \quad \frac{\hbar^2}{2m_0} A_3 = M_2 - L_2, \quad (33)$$

$$\frac{\hbar^2}{2m_0} A_4 = \frac{L_1 + M_1}{2} - M_3, \quad \frac{\hbar^2}{2m_0} A_5 = \frac{N_1}{2}, \quad \frac{\hbar^2}{2m_0} A_6 = \frac{N_2}{\sqrt{2}}.$$

Note that there is a minus sign in front of all the K terms in Eq. (31) and we do not have a factor of i in the definition of the H terms compared with those used in Refs. 7 and 14. We believe that our results are consistent with the fact that both A_5 and A_6 are real constants and that they agree with our results to be derived in Sec. IV, using the invariant method, which is the method used by Pikus and Bir. Fortunately, due to cancellations, these sign changes and the i factor do not affect the band-structure dispersion relation, which was used^{14,15} to fit the more exact band structures to extract these band-edge parameters. They may affect the relative phases of the band-edge wave functions, though.

The strain effects can be easily included by the same symmetry consideration and a straightforward addition of corresponding terms:

$$k_{\alpha} k_{\beta} \rightarrow \epsilon_{\alpha\beta},$$

with the deformation potentials, D_1, D_2, \dots, D_6 , at the corresponding positions of A_1, A_2, \dots, A_6 .

$$\begin{aligned}
F &= \Delta_1 + \Delta_2 + \lambda + \theta, \\
G &= \Delta_1 - \Delta_2 + \lambda + \theta, \\
\lambda &= \frac{\hbar^2}{2m_0} [A_1 k_z^2 + A_2 (k_x^2 + k_y^2)] + \lambda_\epsilon, \\
\lambda_\epsilon &= D_1 \epsilon_{zz} + D_2 (\epsilon_{xx} + \epsilon_{yy}), \\
\theta &= \frac{\hbar^2}{2m_0} [A_3 k_z^2 + A_4 (k_x^2 + k_y^2)] + \theta_\epsilon, \\
\theta_\epsilon &= D_3 \epsilon_{zz} + D_4 (\epsilon_{xx} + \epsilon_{yy}), \\
K &= \frac{\hbar^2}{2m_0} A_5 (k_x + i k_y)^2 + D_5 \epsilon_+, \\
H &= \frac{\hbar^2}{2m_0} A_6 k_z (k_x + i k_y) + D_6 \epsilon_{z+}, \\
\Delta &= \sqrt{2} \Delta_3,
\end{aligned} \tag{34}$$

where

$$\begin{aligned}
\epsilon_\pm &= \epsilon_{xx} \pm 2i \epsilon_{xy} - \epsilon_{yy}, \\
\epsilon_{z\pm} &= \epsilon_{zx} \pm i \epsilon_{yz}.
\end{aligned} \tag{35}$$

It should be pointed out that under the cubic approximation,^{8,14} the following relations hold for the parameters A_i 's and Δ_i 's:

$$\begin{aligned}
A_1 - A_2 &= -A_3 = 2A_4, \quad A_3 + 4A_5 = \sqrt{2}A_6, \quad \Delta_2 = \Delta_3, \\
D_1 - D_2 &= -D_3 = 2D_4, \quad D_3 + 4D_5 = \sqrt{2}D_6.
\end{aligned} \tag{36}$$

Therefore, only five band-structure parameters, such as A_1 , A_2 , A_5 , Δ_1 , and Δ_2 , and three deformation potentials are necessary for the calculation of the valence-band structures. The cubic approximation idea is based on the similarity between the wurtzite structure and the cubic crystal. The above relations are derived⁸ if we map the c (0001) axis to the z' axis along the (111) direction and set the x' and y' axes along the $[\bar{1}12]$ and $[\bar{1}10]$ directions, respectively, in the coordinate system. It has also been found^{8,14} that a seventh coefficient A_7 for the linear k terms vanishes; therefore, we discard it at the beginning and keep only the quadratic terms of k , in addition to the band-edge energy terms.

For a strained-layer wurtzite crystal pseudomorphically grown along the (0001) (z axis) direction, the strain tensor $\bar{\epsilon}$ has only the following nonvanishing diagonal elements:

$$\begin{aligned}
\epsilon_{xx} = \epsilon_{yy} &= \frac{a_0 - a}{a}, \\
\epsilon_{zz} &= -\frac{2C_{13}}{C_{33}} \epsilon_{xx},
\end{aligned} \tag{37}$$

where a_0 and a are the lattice constants of the substrate and the layer material, and C_{13} and C_{33} are the stiffness con-

stants. The general strain-stress relation (Hooke's Law) for the hexagonal crystal can be found in Ref. 29.

IV. THE INVARIANT METHOD FOR THE EFFECTIVE-MASS HAMILTONIAN

Using the Hamiltonian for a strained wurtzite structure based on the symmetry consideration, we write

$$\begin{aligned}
H &= \Delta_1 J_z^2 + \Delta_2 J_z \sigma_z + \Delta (J_+ \sigma_- + J_- \sigma_+) \\
&\quad + \frac{\hbar^2}{2m_0} [(A_1 + A_3 J_z^2) k_z^2 + (A_2 + A_4 J_z^2) (k_x^2 + k_y^2) \\
&\quad - A_5 (J_+^2 k_-^2 + J_-^2 k_+^2) - 2A_6 k_z ([J_z J_+] k_- + [J_z J_-] k_+)] \\
&\quad + (D_1 + D_3 J_z^2) \epsilon_{zz} + (D_2 + D_4 J_z^2) (\epsilon_{xx} + \epsilon_{yy}) \\
&\quad - D_5 (J_+^2 \epsilon_- + J_-^2 \epsilon_+) - 2D_6 ([J_z J_+] \epsilon_{z-} + [J_z J_-] \epsilon_{z+}),
\end{aligned} \tag{38}$$

where

$$\begin{aligned}
J_\pm &= \frac{1}{\sqrt{2}} (J_x \pm i J_y), \\
\sigma_\pm &= \frac{1}{2} (\sigma_x \pm i \sigma_y),
\end{aligned} \tag{39}$$

$$2[J_z J_\pm] = J_z J_\pm + J_\pm J_z,$$

and we have specified the bases, $\{Y_{11}, Y_{10}, \text{ and } Y_{1-1}\}$, with the operator matrices, J_x, J_y, J_z , and the Pauli spin matrices explicitly defined in Appendix A. It should be noted that because of the changes in the basis functions involving changes of signs and phase factors in early and recent papers, confusion occurred in deriving the Hamiltonian matrix. Since the previous derivations for the wurtzite Hamiltonian were based on the invariant method, the sign and the phase factor in front of the A_5 and A_6 (or the H and K terms) were arbitrarily chosen as long as the Hamiltonian stays Hermitian. A consistent approach is to derive the Hamiltonian using the $\mathbf{k} \cdot \mathbf{p}$ method, as shown in Sec. III.

In writing the Hamiltonian, we have kept in mind that the band-structure parameters $A_i, i=1,2,3, \dots, 6$, are all real numbers, following our definitions using the $\mathbf{k} \cdot \mathbf{p}$ method. The Hamiltonian (38) can also be simplified to the following form:

$$\begin{aligned}
H &= (\Delta_1 + \theta) J_z^2 + \Delta_2 J_z \sigma_z + \lambda \\
&\quad + \Delta (J_+ \sigma_- + J_- \sigma_+) - (K^* J_+^2 + K J_-^2) \\
&\quad - (H^* 2[J_z J_+] + H 2[J_z J_-]),
\end{aligned} \tag{40}$$

where λ, θ, K , and H are the same as those defined in Eq. (34).

In the following bases, $\{Y_{11}\uparrow, Y_{10}\uparrow, Y_{1-1}\uparrow, Y_{11}\downarrow, Y_{10}\downarrow, Y_{1-1}\downarrow\}$, the full six-by-six Hamiltonian matrix can be written as

$$H = \begin{bmatrix} F & -H^* & -K^* & 0 & 0 & 0 \\ -H & \lambda & H^* & \Delta & 0 & 0 \\ -K & H & G & 0 & \Delta & 0 \\ 0 & \Delta & 0 & G & -H^* & -K^* \\ 0 & 0 & \Delta & -H & \lambda & H^* \\ 0 & 0 & 0 & -K & H & F \end{bmatrix} \begin{matrix} |Y_{11}\uparrow\rangle (=|u_1\rangle) \\ |Y_{10}\uparrow\rangle (=|u_3\rangle) \\ |Y_{1-1}\uparrow\rangle (=|u_2\rangle) \\ |Y_{11}\downarrow\rangle (=|u_5\rangle) \\ |Y_{10}\downarrow\rangle (=|u_6\rangle) \\ |Y_{1-1}\downarrow\rangle (=|u_4\rangle) \end{matrix}. \quad (41)$$

This result, when written in the same order of the bases $\{u_1, u_2, \dots, u_6\}$, gives an identical result as that in Eq. (31), which was derived from the second-order $\mathbf{k} \cdot \mathbf{p}$ method taking the symmetry of wurtzite crystals into consideration.

It should be pointed out that some sign changes in the choice of bases are possible, such that the original definitions of the K and H terms of Pikus and Bir can still be used. For example, using $\{-u_1, u_2, iu_3, u_4, -u_5, iu_6\}$, we find a sign change in front of K and an extra factor of i in both H and Δ . In this set of bases, the complete Hamiltonian matrix differs from the original form in Ref. 8, only by an extra i factor in front of Δ . We believe that our formulation gives consistent results based on both the Luttinger-Kohn model and the invariant method.

V. BLOCK-DIAGONALIZATION AND THE VALENCE-BAND DISPERSIONS

The full six-by-six Hamiltonian matrix can be block diagonalized following a similar procedure^{26,30} to that of the zinc-blende structure. We note that the off-diagonal terms such as K and H contain the ϕ dependence and write

$$\begin{aligned} K &= K_t e^{2\phi}, & K_t &= \frac{\hbar^2}{2m_0} A_5 k_t^2; \\ H &= H_t e^{i\phi}, & H_t &= \frac{\hbar^2}{2m_0} A_6 k_t k_z, \end{aligned} \quad (42)$$

where $k_x + ik_y = k_t \exp(i\phi)$ has been used. First, it is easy to see that we can remove the ϕ dependence in the matrix elements by introducing the bases, $\{\exp(-i3\phi/2)|Y_{11}\uparrow\rangle, \exp(i\phi/2)|Y_{1-1}\uparrow\rangle, \exp(-i\phi/2)|Y_{10}\uparrow\rangle, \exp(i3\phi/2)|Y_{1-1}\downarrow\rangle, \exp(-i\phi/2)|Y_{11}\downarrow\rangle, \exp(i\phi/2)|Y_{10}\downarrow\rangle\}$. By pairing the bases $\{u_1, u_4\}$, $\{u_2, u_5\}$, and $\{u_3, u_6\}$, we form the bases $|1\rangle, |2\rangle, |3\rangle, |4\rangle, |5\rangle$, and $|6\rangle$ by using the basis transformation, $|i\rangle = \sum T_{ij} u_j$, where the T matrix is defined as

$$T = \begin{bmatrix} \alpha^* & 0 & 0 & \alpha & 0 & 0 \\ 0 & \beta & 0 & 0 & \beta^* & 0 \\ 0 & 0 & \beta^* & 0 & 0 & \beta \\ \alpha^* & 0 & 0 & -\alpha & 0 & 0 \\ 0 & \beta & 0 & 0 & -\beta^* & 0 \\ 0 & 0 & -\beta^* & 0 & 0 & \beta \end{bmatrix}, \quad (43)$$

where

$$\alpha = \frac{1}{\sqrt{2}} e^{i(3\pi/4 + 3\phi/2)}, \quad \beta = \frac{1}{\sqrt{2}} e^{i(\pi/4 + \phi/2)}. \quad (44)$$

The Hamiltonian matrix is then block diagonalized, $H' = U H U^\dagger = T^* H T$,

$$H' = \begin{bmatrix} F & K_t & -iH_t & 0 & 0 & 0 \\ K_t & G & \Delta - iH_t & 0 & 0 & 0 \\ iH_t & \Delta + iH_t & \lambda & 0 & 0 & 0 \\ 0 & 0 & 0 & F & K_t & iH_t \\ 0 & 0 & 0 & K_t & G & \Delta + iH_t \\ 0 & 0 & 0 & -iH_t & \Delta - iH_t & \lambda \end{bmatrix}, \quad (45)$$

where the superscript \dagger means taking both transpose (superscript t) and complex conjugate (*). The transformation matrix²⁶ for the components of the wave functions is $U = T^*$. By writing the upper-left Hamiltonian as H^U and the lower-right Hamiltonian as H^L , we find the relation $H^U = (H^L)^* = (H^L)^\dagger$.

VI. ANALYTICAL EXPRESSIONS FOR THE EFFECTIVE MASSES AND OPTICAL MOMENTUM-MATRIX ELEMENTS

The effective masses along the transverse and longitudinal directions can be derived as follows:

(i) Near the zone center (k approaches zero), we keep

TABLE I. Normalized inverse effective masses of the heavy-hole (HH), light-hole (LH), and crystal-field split hole (CH) bands along the c axis ($=z$ axis) and transverse (t) to the c axis.

Valence energy	m_0/m^z	m_0/m^t
Near the band edge ($k \rightarrow 0$)		
E_1 (HH band)	$-(A_1 + A_3)$	$-(A_2 + A_4)$
E_2 (LH band)	$- \left[A_1 + \frac{(E_2^0 - \lambda_\epsilon)}{E_2^0 - E_3^0} A_3 \right]$	$- \left[A_2 + \frac{(E_2^0 - \lambda_\epsilon)}{E_2^0 - E_3^0} A_4 \right]$
E_3 (CH band)	$- \left[A_1 + \frac{(E_3^0 - \lambda_\epsilon)}{E_3^0 - E_2^0} A_3 \right]$	$- \left[A_2 + \frac{(E_3^0 - \lambda_\epsilon)}{E_3^0 - E_2^0} A_4 \right]$
Far away from the band edge (k is large)		
E_1 (HH band)	$-(A_1 + A_3)$	$-(A_2 + A_4 - A_5)$
E_2 (LH band)	$-(A_1 + A_3)$	$-(A_2 + A_4 + A_5)$
E_3 (CH band)	$-A_1$	$-A_2$

only terms of up to the second order in k and find (for a finite $\Delta_i, i=1,2,3$)

$$E_1 = F,$$

$$E_2 = \frac{G+\lambda}{2} + \sqrt{\left(\frac{G-\lambda}{2}\right)^2 + \Delta^2}, \quad (46)$$

$$E_3 = \frac{G+\lambda}{2} - \sqrt{\left(\frac{G-\lambda}{2}\right)^2 + \Delta^2}.$$

The band-edge effective masses along the longitudinal ($z=c$ axis) and the transverse (x or y) directions can then be obtained and are tabulated in Table I. Using the band-edge wave functions (11), we also obtain the momentum-matrix elements in Table II for the optical transition from the conduction band edge to the three valence-subband edges (C-HH, C-LH, and C-CH transitions labeled as E_1 , E_2 , and E_3 , respectively), when the optical polarization is parallel or perpendicular to the c axis. Our analytical results including

TABLE II. Strain-dependent interband momentum-matrix elements $|\langle S|\hat{\mathbf{e}} \cdot \mathbf{p}|v_i \rangle|^2$ for $\hat{\mathbf{e}}$ polarizations along the c axis ($=z$) and perpendicular to the c axis. The band-edge wave functions v_i are listed in Eq. (11). Here, the energy parameters for the interband transition elements are related to Kane's parameters, P_1 and P_2 in Eq. (18), by $E_{pz} = (2m_0/\hbar^2)P_1^2$ and $E_{px} = (2m_0/\hbar^2)P_2^2$. Note that $a^2 + b^2 = 1$; a and b are defined in Eq. (48).

Valence energy	$\hat{\mathbf{e}} \parallel c$ axis	$\hat{\mathbf{e}} \perp c$ axis
E_1 (HH band)	0	$\frac{m_0}{4} E_{px}$
E_2 (LH band)	$b^2 \left(\frac{m_0}{2} E_{pz} \right)$	$a^2 \left(\frac{m_0}{4} E_{px} \right)$
E_3 (CH band)	$a^2 \left(\frac{m_0}{2} E_{pz} \right)$	$b^2 \left(\frac{m_0}{4} E_{px} \right)$
Sum	$\frac{m_0}{2} E_{pz}$	$\frac{m_0}{2} E_{px}$

the strain effects in Tables I and II are simple and useful, where E_1^0 , E_2^0 , and E_3^0 , are the band-edge energies, E_1 , E_2 , E_3 in Eq. (46), evaluated at $\mathbf{k}=\mathbf{0}$,

$$E_1^0 = \Delta_1 + \Delta_2 + \theta_\epsilon + \lambda_\epsilon,$$

$$E_2^0 = \frac{\Delta_1 - \Delta_2 + \theta_\epsilon}{2} + \lambda_\epsilon + \sqrt{\left(\frac{\Delta_1 - \Delta_2 + \theta_\epsilon}{2}\right)^2 + 2\Delta_3^2}, \quad (47)$$

$$E_3^0 = \frac{\Delta_1 - \Delta_2 + \theta_\epsilon}{2} + \lambda_\epsilon - \sqrt{\left(\frac{\Delta_1 - \Delta_2 + \theta_\epsilon}{2}\right)^2 + 2\Delta_3^2}.$$

We also redefine Eq. (12) to include the strain effects,

$$a = \frac{E_2^0 - \lambda_\epsilon}{\sqrt{(E_2^0 - \lambda_\epsilon)^2 + 2\Delta_3^2}},$$

$$b = \frac{\sqrt{2}\Delta_3}{\sqrt{(E_2^0 - \lambda_\epsilon)^2 + 2\Delta_3^2}}, \quad (48)$$

and it is straightforward to show that

$$a^2 = \frac{E_2^0 - \lambda_\epsilon}{E_2^0 - E_3^0}, \quad b^2 = \frac{E_3^0 - \lambda_\epsilon}{E_3^0 - E_2^0},$$

which are used in Tables I and II.

The conduction-band edge has a hydrostatic energy shift, $P_{c\epsilon}$,

$$E_c = E_v^0 + \Delta_1 + \Delta_2 + E_g + P_{c\epsilon},$$

$$P_{c\epsilon} = a_{cz}\epsilon_{zz} + a_{ct}(\epsilon_{xx} + \epsilon_{yy}). \quad (49)$$

For a GaN layer sandwiched between two thick $\text{Al}_x\text{Ga}_{1-x}\text{N}$ layers, the strain is compressive in nature, since the lattice constant a of the GaN layer before deformation is larger than the lattice constant a_0 of $\text{Al}_x\text{Ga}_{1-x}\text{N}$ layers. Therefore, ϵ_{xx} is negative, and the band-edge shifts will be positive for the conduction band and negative for the top valence bands. The net band-gap shift is determined by

$$E_c - E_1^0 = E_g + P_{c\epsilon} - (\theta_\epsilon + \lambda_\epsilon), \quad (50)$$

and it can be compared with the lowest band-edge transition energy (A line) of the photoluminescence spectrum, with an exciton correction energy of about 28 meV. Similarly, $E_c - E_2^0$ and $E_c - E_3^0$ with the same exciton correction can be used to compare with the transition energies of the B and C lines in the photoluminescence spectrum.

(ii) Away from the zone center, as k approaches a big number, we can ignore Δ_2 and Δ_3 ; the rest of the Hamiltonian has analytical solutions:

$$E_1 = F' - K_t,$$

$$E_2 = \frac{1}{2} [F' + K_t + \lambda + \sqrt{(F' + K_t - \lambda)^2 + 8H_t^2}], \quad (51)$$

$$E_3 = \frac{1}{2} [F' + K_t + \lambda - \sqrt{(F' + K_t - \lambda)^2 + 8H_t^2}],$$

where $F' = \Delta_1 + \lambda + \theta$. Using the above expressions, the valence-band effective masses away from the zone center can be obtained analytically and are tabulated in Table I. Note that in the special case of $\Delta_2 = \Delta_3 = 0$, these analytical effective masses are the exact solutions of the three-by-three Hamiltonians H^U and H^L . The above analysis also explains the difference between the expressions for the effective masses used in Refs. 8 and 14.

VII. NUMERICAL EXAMPLES

For a special case, if we ignore the anisotropic property of the wurtzite crystals, we can assume that $a_{cz} = a_{ct} = a_c$. Since the experimental data only provide the total band-gap shift as a function of an externally applied pressure, only the total value for the interband deformation potential, a , is reported. Theoretically, the hydrostatic deformation potentials $a = \partial E_g / \partial (\ln V) = a_c - a_v$ (interband), a_c (conduction band), a_v (valence band), and the shear deformation potential, b , have been used for zinc-blende structures. Possible rules for the partition ratio, $|a_c/a|$ and $|a_v/a|$, are used based on different theories. Note that the common convention that a and a_c are negative and a_v is positive is used. For wurtzite structure, the parameters, D_1 and D_2 , play similar roles²³ as the hydrostatic deformation potential, a_v ; while D_3 and D_4 play similar roles as the shear deformation potential, b , of cubic crystals. Various values of a for GaN, such as^{13,22} -7.8 , -9.2 , and -11.8 eV have been reported. A set of parameters, using $a = -8.16$ eV, $a_c = 0$, $D_1 = D_2 = 8.16$ eV, $D_3 = D_4 = -3.71$ eV, $\Delta_1 = 10$ meV, $\Delta_2 = 6.2$ meV, and $\Delta_3 = 5.5$ meV have been used²³ to fit experimental data collected from a few samples for temperatures lower than 10 K. Note that these parameters were obtained by a linearization of the valence-band-edge energies with respect to strain. We have used the same parameters to calculate the transition energies (with exciton corrections) for the A-line, B-line, and C-line interband transitions in the photoluminescence spectrum using the exact expressions, (47) and (49), instead of the linearization formulas. The results are shown as the dashed lines in Fig. 3, while the data points collected in Ref. 23 are shown as symbols. We have used

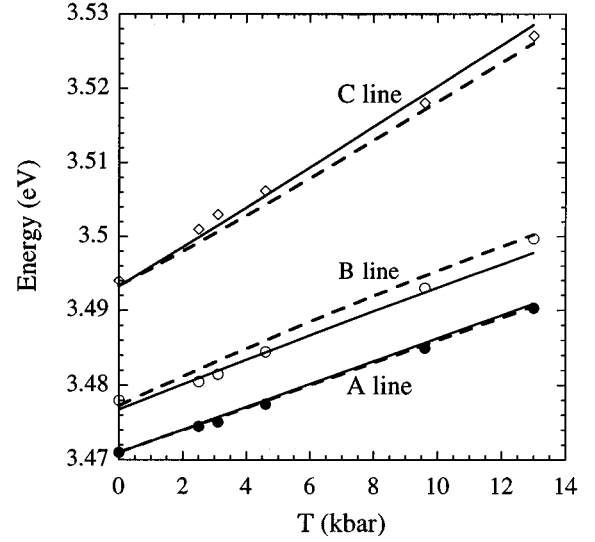


FIG. 3. Interband energies calculated for the transitions between the conduction band E_c and the HH, LH, and CH bands, or called A, B, and C lines. The symbols are experimental data from GaN samples at temperatures below 10 K collected in Ref. 23. The solid lines are calculated using the parameters in Table III in expressions in Eq. (47) for E_1^0 , E_2^0 , and E_3^0 , and E_c in Eq. (49) with an exciton energy ($E_{\text{ex}} \approx 0.028$ eV) correction [$E_g(10 \text{ K}) - E_{\text{ex}} \approx 3.471$ eV]. The dashed lines are calculated using the same equations with parameters taken from Ref. 23.

$\epsilon_{xx} = -[C_{11} + C_{12} - 2(C_{13}^2/C_{33})]^{-1}T$ and T is the magnitude of the equivalent in-plane compressive stress in kbar. It is noted that the fit is not unique, since the roots for Δ_{cr} and Δ_{so} are symmetric, as can be seen from Eqs. (14). It is usually believed that $\Delta_{\text{cr}} \geq \Delta_{\text{so}} = 3\Delta_2$; and $\Delta_{\text{cr}} = 22$ meV, $\Delta_{\text{so}} = 11$ meV, have been used. These values affect the magnitudes of E_1^0 , E_2^0 , E_3^0 , and the polarization selection rules for optical transitions between the conduction band and the LH (E_2^0) and CH (E_3^0) valence bands. We have varied the parameters using $\Delta_1 = 16$ meV, $\Delta_2 = \Delta_3 = 4$ meV and found that our fit with the data in Fig. 3 is within 2 meV. Our parameters will not reverse the polarization selection rule compared with previous report,²⁷ while the Δ_i parameters of Ref. 23 will have different polarization selection rules for the B and C lines of the photoluminescence spectrum from those in Ref. 27. More experimental data on the polarization selection rules, especially near the B and C lines of the interband transitions, are required to resolve this issue. We then changed the deformation potentials: $a_c = 0.5a = -4.08$ eV, $D_1 = 0.7$ eV, $D_2 = 2.1$ eV, $D_3 = 1.4$ eV, and $D_4 = -0.7$ eV, and obtain the solid lines in Fig. 3. These parameters satisfy the cubic approximation, $D_1 - D_2 = -D_3 = 2D_4$. There are few reports on the experimental values of a_c and D_i s, since these parameters cannot be independently measured so far. The above values are of the same magnitudes as the hydrostatic and shear deformation potentials of the other III-V zinc-blende crystals.

In Figs. 4(a) and (b), we plot the band-edge energy shifts for the conduction band and the three valence bands as a function of the in-plane compressive strain up to a strain value of a magnitude 0.01 (or one percent). Note that we use the convention ϵ_{xx} to be negative for a biaxial compression case. One percent of compressive strain is the amount of the

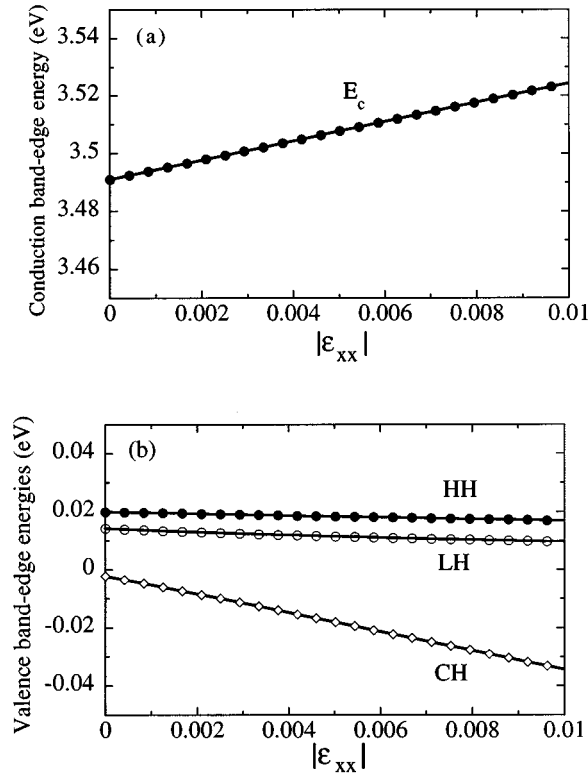


FIG. 4. Strain effects on (a) the conduction- and (b) the valence-band energy shifts are illustrated based on our model and the partition rules for the hydrostatic deformation potentials. Note that the band-gap energy $E_c - E_1$ increases linearly with the in-plane compressive strain.

in-plane strain in a GaN quantum well sandwiched between two $\text{Al}_x\text{Ga}_{1-x}\text{N}$ layers with an aluminum mole fraction $x \approx 0.4$.

In Fig. 5, we show the band-edge valence-band structure of a -1% compressively strained GaN wurtzite crystal. The valence-band energy is plotted as a two-dimensional function of k_t ($=k_x$ or k_y) and k_z . The effective-mass parameters, A_i 's, and the energy splitting parameters, Δ_i 's, have been calculated by fitting the more accurate electronic band structures calculated using first principles.¹⁴ Here, we use the same effective-mass parameters as in Ref. 14 and the deformation potentials from our fit in Fig. 3. All parameters are listed in Table III. It should be noted that more theoretical and experimental work is needed to determine all these parameters consistently. The parameters listed in Table III can only serve as a guide for our theoretical modeling. Our chosen set of parameters have been used to fit the data in Fig. 3 very well. The bulk valence-band structure for an unstrained GaN wurtzite crystal has been shown in Fig. 1(a) of Ref. 17 with the same set of parameters. A comparison between Fig. 5 and the unstrained valence-band structure shows that the strain effects shift the HH and LH band edges by an almost equal amount, and shift the CH band away from the zone center.

The difference in symmetry between the wurtzite and zinc-blende structures causes some fundamental differences in their electronic and optical properties. The degeneracy between the heavy-hole and light-hole bands at the zone center (Γ point) for the zinc-blende structure is broken for the

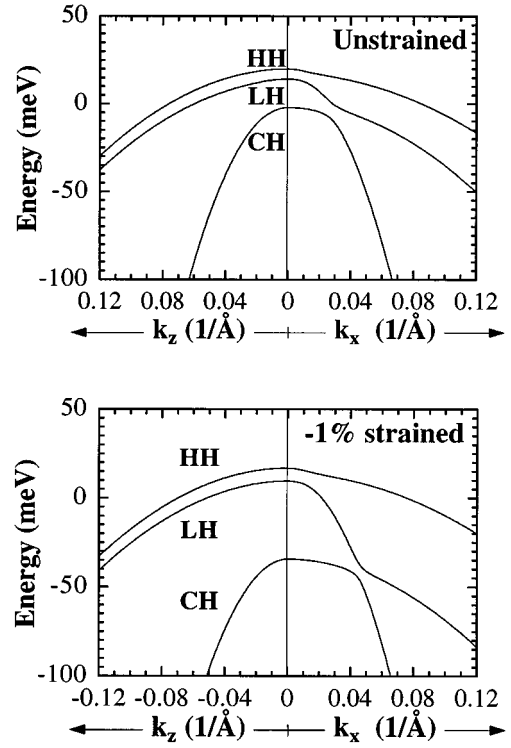


FIG. 5. Valence-band dispersions for an unstrained a -1% compressively strained GaN wurtzite crystal. The vertical axis is the valence-band energy and the horizontal axes are the transverse k_x and longitudinal $k_z = c(0001)$ axes.

wurtzite structure. For a zinc-blende layer grown along the (001) direction with a compressive strain, the deformation potentials lift the HH band up and reduce its in-plane effective mass. However, for a wurtzite layer grown along the c axis, the compressive strain shifts both the HH and LH bands by almost the same amount and the in-plane effective masses remain almost the same as those in the unstrained case. The polarization selection rules for the conduction band to the light-hole band are also changed. For the zinc-blende structure, the dominant C-LH transitions are TM polarization (along the growth axis). However, for the wurtzite structure, TE polarization is favored for the C-LH transitions.

In Fig. 6, the band-edge hole effective masses of a biaxial compressively strained GaN along the longitudinal (z) and transverse (t) directions listed in Table I are calculated as a function of the magnitude of the in-plane compressive strain. For example, in the absence of strain, the band-edge effective masses are

$$\begin{aligned} m_{\text{hh}}^z/m_0 &= 1.10, & m_{\text{hh}}^t/m_0 &= 0.27, \\ m_{\text{lh}}^z/m_0 &= 0.60, & m_{\text{lh}}^t/m_0 &= 0.30, \\ m_{\text{ch}}^z/m_0 &= 0.17, & m_{\text{ch}}^t/m_0 &= 0.77. \end{aligned}$$

From Figs. 5 and 6, we can see that the HH and LH bands near the band edges have very similar effective masses in the k_t direction. However, in the k_z direction, HH has a heavier effective mass than that of the light hole (both masses are heavy). On the other hand, far away from the zone center, the HH band has a heavier effective mass than that of the LH

TABLE III. Physical parameters for GaN and AlN.

Parameter	GaN	AlN
Lattice constant ^{a-c} (Å)		
a	3.1892	3.112
c	5.1850	4.982
Energy parameters ^{a-f}		
E_g (eV) at 300 K	3.44	6.28
$\Delta_1 = \Delta_{cr}$ (meV)	16 (this work)	-58.5 ^f
	10 ^d	
	22 ^e	
Δ_{so} (meV)	12 (this work)	
	11 ^e	
$\Delta_2 = \Delta_{so}/3$ (meV)	4 (this work)	6.80 ^f
	6.2 ^d	
	3.7 ^e	
Δ_3 (meV)	4 (this work)	6.80 ^f
	5.5 ^d	
	3.7 ^e	
Conduction-band effective masses ^f		
m_e^z/m_0	0.20	0.33
m_e^t/m_0	0.18	0.25
Valence band effective-mass parameters ^f		
A_1	-6.56	-3.95
A_2	-0.91	-0.27
A_3	5.65	3.68
A_4	-2.83	-1.84
A_5	-3.13	-1.95
A_6	-4.86	-2.91
Deformation potentials (eV)		
a (interband)	-8.16 ^e	
$a_c = 0.5a$	-4.08 (this work)	
D_1	0.7 (this work)	
D_2	2.1 (this work)	
D_3	1.4 (this work)	
D_4	-0.7 (this work)	
Elastic stiffness constants ^{a,b} (10^{11} dyn/cm ²)		
C_{13}	15.8	12.0
C_{33}	26.7	39.5

^aReference 31.^bReference 32.^cReference 33.^dReference 23.^eReference 27.^fReference 14.

band along the k_t direction, and they have similar effective masses in the k_z direction. Since Δ_2 and Δ_3 are small, the band structures appear to be dominated by the features determined by the effective masses away from the zone center. This suggests that for a GaN quantum-well structure, the heavy-hole and light-hole subband energies will be very close and the density of states for the heavy-hole subbands will be much larger than that for the light-hole subbands.

The normalized matrix elements for the optical transitions from the conduction band to the HH, LH, and CH bands are plotted as a function of the in-plane strain, as shown in Fig. 7 for the optical polarization ($\hat{\mathbf{e}}$) parallel to the c (z) axis (TM polarization) and perpendicular to the c axis (TE polar-

ization). The analytical expressions are tabulated in Table II. We also calculate the energy parameters for the interband optical-transition oscillator strengths and obtain $E_{px} = 15.7$ eV, and $E_{pz} = 13.9$ eV. Notice the sum rules for each polarization in Table II. All the matrix elements are normalized to the total value for the TE polarization. The sum of all three transitions, C-HH, C-LH, and C-CH, for the TE polarization is unity, and the sum of all three matrix elements for the TM polarization is $E_{pz}/E_{px} = 0.89$.

VIII. CONCLUSIONS

In conclusion, we have derived the effective Hamiltonian for the wurtzite crystals using both the $\mathbf{k} \cdot \mathbf{p}$ method and the

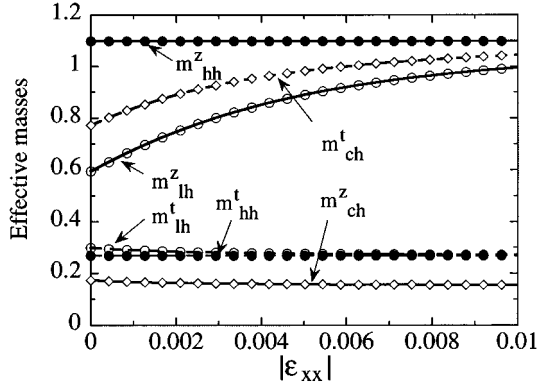


FIG. 6. The effective masses (m^z/m_0 and m^t/m_0) near the band edges calculated using the analytical expressions in Table I as a function of the in-plane compressive strain are plotted for the HH, LH, and CH bands.

invariant method. We show the explicit definitions of the fundamental band-structure parameters, the interband momentum-matrix elements, and the energy parameters. A unitary transformation is also found to block diagonalize the six-by-six matrix into two three-by-three matrices and it simplifies the derivations for the valence-band dispersions and effective masses. Analytical expressions for the effective masses near and far away from the band edges and the band-edge wave functions are derived within the framework of the $\mathbf{k}\cdot\mathbf{p}$ method. Analytical expressions and numerical results for the effective masses and optical interband transition matrix elements taking into account the strain effects have also been presented. This Hamiltonian will be very useful for the calculation of both electronic and optical properties of strained bulk and quantum-well structures, using GaN/Al_xGa_{1-x}N or In_yGa_{1-y}N/Al_xGa_{1-x}N materials, which have a great potential for applications to blue-green laser diodes and electronic devices.

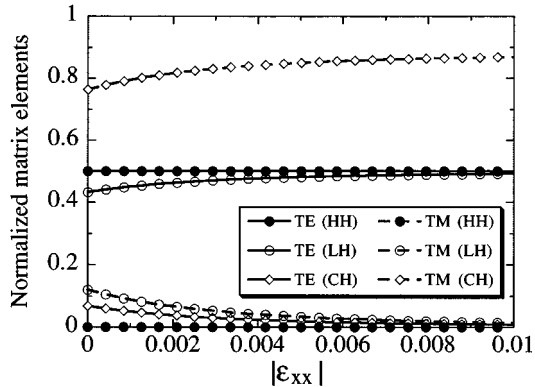


FIG. 7. Normalized interband transition matrix elements as a function of strain are plotted for optical polarization along the c axis (TM polarization) and perpendicular to the c axis (TE polarization). The optical transitions from the conduction band to the HH, LH, and CH bands follow a simple sum rule, as listed in Table II.

ACKNOWLEDGMENTS

This work was supported by the U. S. Office of Naval Research under Grant No. N00014-96-1-0303. S. L. Chuang was also supported by the Center for Advanced Study at the University of Illinois.

APPENDIX A: MATRICES AND BASIS FUNCTIONS

Pauli spin matrices and bases:

$$\sigma_x = \begin{bmatrix} 0 & 1 \\ 1 & 0 \end{bmatrix}, \quad \sigma_y = \begin{bmatrix} 0 & -i \\ i & 0 \end{bmatrix}, \quad \sigma_z = \begin{bmatrix} 1 & 0 \\ 0 & -1 \end{bmatrix}, \quad (\text{A1})$$

in the bases $|\uparrow\rangle$ and $|\downarrow\rangle$. We also use

$$\sigma_+ = \frac{1}{2}(\sigma_x + i\sigma_y) = \begin{bmatrix} 0 & 1 \\ 0 & 0 \end{bmatrix}, \quad \sigma_- = \frac{1}{2}(\sigma_x - i\sigma_y) = \begin{bmatrix} 0 & 0 \\ 1 & 0 \end{bmatrix}. \quad (\text{A2})$$

Angular momentum matrices and bases:

$$J_x = \frac{1}{\sqrt{2}} \begin{bmatrix} 0 & 1 & 0 \\ 1 & 0 & 1 \\ 0 & 1 & 0 \end{bmatrix}, \quad J_y = \frac{1}{\sqrt{2}} \begin{bmatrix} 0 & -i & 0 \\ i & 0 & -i \\ 0 & i & 0 \end{bmatrix},$$

$$J_z = \begin{bmatrix} 1 & 0 & 0 \\ 0 & 0 & 0 \\ 0 & 0 & -1 \end{bmatrix}. \quad (\text{A3})$$

The basis functions are in the following order:

$$Y_{11} = \frac{-1}{\sqrt{2}}|X+iY\rangle, \quad Y_{10} = |Z\rangle, \quad Y_{1-1} = \frac{1}{\sqrt{2}}|X-iY\rangle. \quad (\text{A4})$$

We also use

$$J_+ = \frac{1}{\sqrt{2}}(J_x + iJ_y) = \begin{bmatrix} 0 & 1 & 0 \\ 0 & 0 & 1 \\ 0 & 0 & 0 \end{bmatrix},$$

$$J_- = \frac{1}{\sqrt{2}}(J_x - iJ_y) = \begin{bmatrix} 0 & 0 & 0 \\ 1 & 0 & 0 \\ 0 & 1 & 0 \end{bmatrix}. \quad (\text{A5})$$

APPENDIX B: DERIVATION OF THE RELATION

$$L_1 - M_1 = N_1$$

We write in the following forms:

$$L_1 - M_1 = \langle X|p^x \hat{G} p^x|X\rangle - \langle X|p^y \hat{G} p^y|X\rangle, \quad (\text{B1})$$

$$N_1 = \langle X|p^x \hat{G} p^y|Y\rangle + \langle X|p^y \hat{G} p^x|Y\rangle, \quad (\text{B2})$$

where the operator \hat{G} is defined as

$$\hat{G} = \sum_{\gamma}^B \frac{\hbar^2 |\gamma\rangle \langle \gamma|}{m_0^2 (E_0 - E_{\gamma})}. \quad (\text{B3})$$

The relation between $L_1 - M_1$ and N_1 can be derived using the sixfold symmetry rotation of the crystal and its corresponding character table.⁸ For a 60° rotation symmetry, we use

$$\begin{aligned}\hat{G}' &= \hat{G}, \\ X' &= \frac{1}{2}X + \frac{\sqrt{3}}{2}Y, \quad Y' = -\frac{\sqrt{3}}{2}X + \frac{1}{2}Y, \\ p^{x'} &= \frac{1}{2}p^x + \frac{\sqrt{3}}{2}p^y, \quad p^{y'} = -\frac{\sqrt{3}}{2}p^x + \frac{1}{2}p^y,\end{aligned}\quad (\text{B4})$$

in

$$L_1 - M_1 = \langle X' | p^{x'} \hat{G}' p^{x'} | X' \rangle - \langle X' | p^{y'} \hat{G}' p^{y'} | X' \rangle. \quad (\text{B5})$$

We obtain

$$L_1 - M_1 = \frac{4}{16}(L_1 - M_1) + \frac{6}{16}(N_1 + N_1^*). \quad (\text{B6})$$

Therefore,

$$L_1 - M_1 = N_1, \quad (\text{B7})$$

since N_1 is real. The relation (B7) is important, since it relates the Hamiltonian (31) derived using the $\mathbf{k} \cdot \mathbf{p}$ method to that derived in the invariant method.

-
- ¹S. Nakamura, T. Mukai, and M. Senoh, *Jpn. J. Appl. Phys.* **30**, L1998 (1991).
²S. Nakamura, T. Mukai, and M. Senoh, *Appl. Phys. Lett.* **64**, 1687 (1994).
³X. H. Yang, T. J. Schmidt, W. Shan, J. J. Song, and B. Goldenberg, *Appl. Phys. Lett.* **66**, 1 (1995).
⁴S. T. Kim, H. Amano, I. Akasaki, and N. Kiode, *Appl. Phys. Lett.* **64**, 1535 (1994).
⁵H. Amano, T. Tanaka, Y. Kunii, K. Kato, S. T. Kim, and I. Akasaki, *Appl. Phys. Lett.* **64**, 1377 (1994).
⁶W. Fang and S. L. Chuang, *Appl. Phys. Lett.* **67**, 751 (1995).
⁷G. E. Pikus, *Zh. Éksp. Teor. Fiz.* **14**, 1075 (1962) [*Sov. Phys. JETP* **14**, 898 (1962)].
⁸G. L. Bir and G. E. Pikus, *Symmetry and Strain-Induced Effects in Semiconductor* (Wiley, New York, 1974).
⁹W. Y. Ching and B. N. Harmon, *Phys. Rev. B* **34**, 5305 (1986).
¹⁰C. Y. Yeh, Z. W. Lu, S. Froyen, and A. Zunger, *Phys. Rev. B* **46**, 10 086 (1992).
¹¹B. J. Min, C. T. Chan, and K. M. Ho, *Phys. Rev. B* **45**, 1159 (1992).
¹²A. Rubio, J. L. Corkill, M. L. Cohen, E. L. Shirley, and S. G. Louie, *Phys. Rev. B* **48**, 11 810 (1993).
¹³M. E. Christensen and I. Gorczyca, *Phys. Rev. B* **50**, 4397 (1994).
¹⁴M. Suzuki, T. Uenoyama, and A. Yanase, *Phys. Rev. B* **52**, 8132 (1995).
¹⁵S. Kamiyama, K. Ohnaka, M. Suzuki, and T. Uenoyama, *Jpn. J. Appl. Phys.* **34**, L821 (1995).
¹⁶T. Uenoyama and M. Suzuki, *Appl. Phys. Lett.* **67**, 2527 (1995).
¹⁷S. L. Chuang and C. S. Chang, *Appl. Phys. Lett.* **68**, 1657 (1996).
¹⁸A. Rubio, J. L. Corkill, and M. L. Cohen, *Phys. Rev. B* **49**, 1952 (1994).
¹⁹J. Neugebauer and C. G. Van de Walle, *Phys. Rev. B* **51**, 10 568 (1995).
²⁰A. Rubio and M. L. Cohen, *Phys. Rev. B* **51**, 4343 (1995).
²¹S.-H. Wei and A. Zunger, *Phys. Rev. Lett.* **76**, 664 (1996).
²²W. Shan, T. J. Schmidt, X. H. Yang, S. J. Hwang, J. J. Song, and B. Goldenberg, *Appl. Phys. Lett.* **66**, 985 (1995); W. Shan *et al.*, *ibid.* **66**, 3492 (1995).
²³B. Gil, O. Briot, and R.-L. Aulombard, *Phys. Rev. B* **52**, R17 028 (1995).
²⁴E. O. Kane, *J. Phys. Chem. Solids* **1**, 249 (1957).
²⁵J. M. Luttinger and W. Kohn, *Phys. Rev.* **97**, 869 (1955).
²⁶S. L. Chuang, *Physics of Optoelectronic Devices* (Wiley, New York, 1995).
²⁷R. Dingle, D. D. Sell, S. E. Stokowski, and M. Ilegems, *Phys. Rev. B* **4**, 1211 (1971).
²⁸P. Löwdin, *J. Phys. Chem.* **19**, 1396 (1951).
²⁹A. E. H. Love, *A Treatise on the Mathematical Theory of Elasticity* (Dover, New York, 1944), pp. 151–160.
³⁰C. Y.-P. Chao and S. L. Chuang, *Phys. Rev. B* **46**, 4110 (1992).
³¹*Physics of Group IV Elements and III-V Compounds*, edited by K. H. Hellwege and O. Madelung, Landolt-Börnstein New Series, Group III, Vol. 17, Pt. a (Springer-Verlag, Berlin, 1982).
³²*Properties of Group III Nitrides*, edited by J. H. Edgar (INSPEC, IEE, London, 1994).
³³S. Strite and H. Morkoç, *J. Vac. Sci. Technol. B* **10**, 1237 (1992).